Nuclear Dynamics and Electronic Transition in a Photosynthetic Reaction Center

Marc Souaille[†] and Massimo Marchi*[,‡]

Contribution from the Centre Européen de Calcul Atomique et Moleculaire (CECAM), Ecole Normale Superieure de Lyon, 46 Allée d'Italie, 69364 Lyon, France, and Section de Biophysique des Protéines et des Membranes, DBCM, DSV, CEA, Centre d'Études, Saclay, 91191 Gif-sur-Yvette Cedex, France

Received November 28, 1994. Revised Manuscript Received December 4, 1996[⊗]

Abstract: This paper is concerned with issues related to the coupling between low-ffrequency nuclear modes and electronic emission in the bacterial reaction center of *Rhodobacter sphaeroides*. We have investigated the temporal evolution of the stimulated emission spectra of the excited state of the special pair bacteriochlorophyll dimer by means of computer simulation. To this purpose, we have carried out molecular dynamics simulations on a hydrated reaction center with the special pair in its ground and excited states, P and P*, respectively. Calculations of the time-dependent stimulated emission spectra has revealed an oscillatory behavior which is consistent with experiments (Vos *et al*.; *Nature* **1993**, *363*, 320; *Biochemistry* **1994**, *33*, 6750). The time scales of these nuclear vibrations are similar to those found experimentally. To a good approximation, both the protein environment and the special pair dimer couple to the P* → P transition with oscillations of similar frequencies. This finding offers an insight on the nature of the nuclear oscillations and might have important implications for their complete understanding.

I. Introduction

The determination of a high-resolution X-ray structure for the RC protein of the purple bacteria *Rhodopseudomonas (Rps.) viridis*[1] and *Rhodobacter (Rb.) sphaeroides*[2−4] has provided a unique opportunity for studying photosynthesis at an atomic level. These proteins constitute an ideal material to investigate phenomena such as electron and proton transfer, the understanding of which is not only relevant to light-driven ET systems of higher plants, but also to all membrane-bound proton motive ET systems.

In the purple bacteria *Rb. sphaeroides*, the RC is composed of chromophores (pigments) and three protein polypeptides (L, M, and H), two of which (L and M) provide the necessary scaffolding to hold the chromophores in place. The third polypeptide (H) is not required for charge separation, but is essential for the correct assembly of the RC and its interaction with the light-harvesting complex which funnel excitations to the primary donor.

The pigment molecules include four bacteriochlorophyll-*a* (B), two bacteriopheophytin-*a* (H), and two quinone molecules. Two bacteriochlorophylls are in van der Waals contact and constitute the primary donor for ET (P). The two subunits L and M are related by a 2-fold symmetry axis, which runs from the center of P to the non-heme iron, on the other side of the membrane. The remaining pigments are organized as two potential branches of electron carriers related by this symmetry axis (so-called L and M) (see Figure 1).

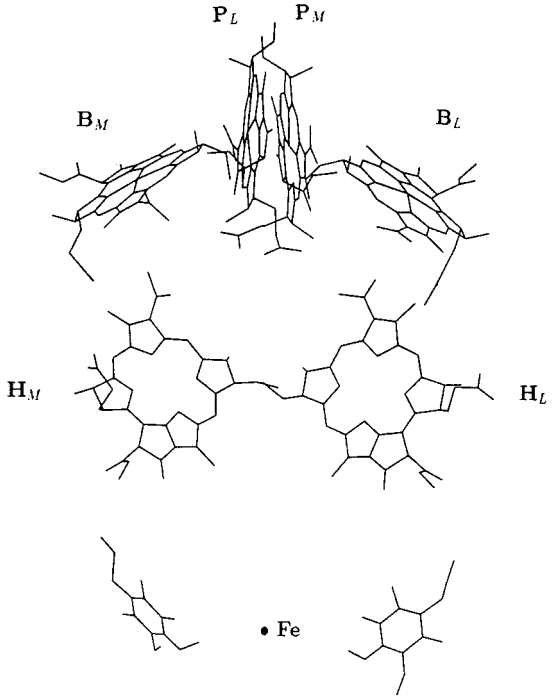

Figure 1. View of the chromophores in the photosynthetic reaction center taken from the X-ray coordinates of *Rhodobacter sphaeroides*.[3] The picture shows on the top, the chromophores involved in the primary charge separation: the so-called special pair (P) formed of two bacteriochlorophylls (P_L and P_M) of the M and L branches, the accessory bacteriochlorophylls (B_L and B_M), and the bacteriopheophytins (H_L and H_M). At the bottom are the two quinones and the non-heme iron.

The photosynthetic reaction is initiated by the absorption of a photon which excites the primary donor from its electronic ground state to its singlet excited state, P*. An electron is then transferred from the chromophore excited state to the bacteriopheophytin on the L side, H_L. This is the so-called primary charge separation (for a recent review, see ref 5). The electron is subsequently shuttled to a series of acceptors while the

* To whom correspondence should be addressed.
[†] Ecole Normale Superieure de Lyon.
[‡] Centre d'Études.
[⊗] Abstract published in *Advance ACS Abstracts*, April 1, 1997.

(1) Deisenhofer, J.; Epp, O.; Miki, K.; Huber, R.; Michel, H. *J. Mol. Biol*. **1984**, *180*, 385. Deisenhofer, J.; Michel, H. *EMBO J*. **1989**, *8*, 2169.
(2) Chang, C. H.; Tiede, D. M.; Tang, J.; Smith, U.; Norris, J. R.; Schiffer, M. *FEBS Lett*. **1986**, *205*, 82. Kabbani, E. P.; Chang, C. H.; Tiede, D. M.; Norris, J. R.; Schiffer, M. *Biochemistry* **1991**, *30*, 5361.
(3) Allen, J. P.; Feher, G.; Yeates, T. O.; Komiya, H.; Rees, D. C. *Proc. Natl. Acad. Sci. U.S.A.* **1987**, *84*, 5730.
(4) Ermler, U.; Fritzch, G.; Buchanan, S.; Michel, M. In *Research in Photosynthesis*; Muratu, N., Ed.; Kluwz: Dordrecht, 1992; Vol. 1, p 341.

S0002-7863(94)03841-2 CCC: $14.00

electron-depleted pigment acquires a new electron from a secondary donor.

In recent times, the P → P* transition which occurs before primary charge separation has received a great deal of attention.[6−15] Femtosecond stimulated emission[9−12] and resonant Raman spectroscopy[13−15] have been used to extract information regarding the coupling between the protin nuclear motion and the electronic transition. In a series of papers Vos *et al*. have explored the time evolution of the stimulated emission spectra from the primary donor of the reaction centers of *Rhodobacter (R.) capsulatus*[9,10] and, more recently, of *Rb. sphaeroides*.[11,12] The experiments consisted in probing the stimulated emission intensity at different frequencies near the Q_y absorption band of P. The low-frequency oscillations in the spectra which persisted, at cryogenic temperatures, for several picoseconds were assigned to coherent nuclear vibrations. The modes that appear in this oscillatory behavior are those coupled to the electronic transition. The amplitude of the oscillation reflects the strength of this coupling and the dynamics of the electronic state. In the latest experiments on *Rb. sphaeroides*,[11,12] vibrations with a frequency between 10 and 190 cm^{-1} were found.

Resonant Raman experiments have also shown low-frequency peaks in the same region.[13−15] Comparison between P and the accessory bacteriochlorophyll (B) shows that Raman shifts below 180 cm^{-1} are unique to the special pair and are not found in the spectra of B. Although early semiempirical calculations seem to indicate that intradimer modes would fall into the same frequency range,[16] the assignment of this low-frequency modes to specific nuclear vibration is still an open issue.

It is worth noticing that the nuclear vibration with the lowest frequency detected by femtosecond spectroscopy has the same time scale as the primary charge separation which occurs immediately after the photoexcitation of the special pair.[5] Thus, the knowledge of the nature of this low-frequency mode might be relevant to the mechanism of this electron transfer.

The primary concern of this study is to address the issue of the coupling mechanism between nuclear modes and electronic transition. Molecular dynamic simulations of the hydrated bacterial reaction center of *Rb. sphaeroides* in the ground and excited states of the special pair were carried out to calculate the time-resolved stimulated emission spectra in a different region of the P* → P transition. A simple electrostatic model for the two energy surfaces was used to evaluate the energy gap whose dynamics is straightforwardly related to the observed spectrum.[17]

A few molecular dynamics simulations of bacterial reaction centers have been carried out in the past.[18,19] Recently, this technique has been used to calculate the diabatic surfaces governing the primary charge separation after photoexcitation.[20] Although the relative positioning of the adiabatic surfaces is controversial,[21] the dynamics of the energy gap calculated by molecular dynamics simulation has shown to account for nonexponential relaxation in photosynthetic RCs.[22]

In earlier studies only the atoms within a region close to the chromophores were actually simulated while the remaining ones were either kept fixed or moved according to stochastic forces.[18−20] Although account of hydration effects were included in a few simulations,[18] only crystallization waters were explicitly modeled.[20] The calculations described in this paper represent an improvement of these earlier models. Here, the reaction center is simulated and surrounded by explicit solvation waters with no restraint on the motion of parts of the protein subunits and with full periodic boundary conditions. In addition, our time-dependent functions have been calculated from rather long trajectories preceded by long equilibration periods.

Anticipating the results, we have been able to obtain a time-resolved stimulated emission spectra which shows qualitatively similar features with the measurements of Vos *et al*.[10,11] In particular, we have found that some low-frequency nuclear oscillations strongly couple to the P* to P electronic emission. These vibrations have frequencies which falls in the same time scale as those found experimentally. Noticeably, to a good approximation, both the protein environment and the special pair dimer couple to the P* to P transition with oscillations of similar frequency. This finding might have implications to identify the nature of the nuclear oscillations.

This paper is organized as follows: In section II a simple model for photoexcitation is presented and its implications for the time-resolved stimulated experiment of Vos *et al*. are discussed. Section III deals with atomistic models of the RC and its environment and gives details of the simulation method and parameters. Section IV describes our model for the excited P* state and how the energy gap between P* and P is calculated during the simulation. In section V we present the results of our simulation. We conclude the paper with a discussion.

II. Nuclear Motion and Electronic Transitions

A. A Simple Model for Photoexcitation. The process of photoexcitation from a ground to an excited state of a pigment molecule in contact with a dielectric can be modeled very simply by a two-level system coupled linearly to a fluctuating field of a bath. While the bath is representative of the dielectric nuclear vibrations, the field includes only the nuclear modes coupled to the electronic transition. This coupling with the nuclear vibrations is responsible for the broadening of electronic bands of pigments in solution or in proteins. In the specific case of

(5) Martin, J.-L.; Vos, M. H. *Annu. Rev. Biophys. Biomol. Struct.* **1992**, *21*, 199.
(6) Martin, J.-L.; Breton, J.; Hoff, A. J.; Migus, A.; Antonetti, A. *Proc. Natl. Acad. Sci. U.S.A.* **1986**, *83*, 957.
(7) Du, M.; Rosenthal, S. J.; Xie, X.; DiMagno, T. J.; Schimdt, M.; Hanson, D. K.; Schiffer, M.; Norris, J. R.; Fleming, G. R. *Proc. Natl. Acad. Sci. U.S.A.* **1992**, *89*, 8517.
(8) Hamm, P.; Gray, K. A.; Oesterhelt, D.; Feick, R.; Scheer, H.; Zinth, W. *Biochim. Biophys. Acta* **1993**, *1142*, 99.
(9) Vos, M. H.; Lambry, J.-C.; Robles, S. J.; Youvan, D. C.; Breton, J.; Martin, J.-L. *Proc. Natl. Acad. Sci. U.S.A.* **1991**, *88*, 8885.
(10) Vos, M. H.; Rappaport, F.; Lambry, J.-C.; Breton, J.; Martin, J.-L. *Nature* **1993**, *363*, 320.
(11) Vos, M. H.; Jones, M. R.; Hunter, C. N.; Breton, J.; Lambry, J.-C.; Martin, J.-L. *Biochemistry* **1994**, *33*, 6750.
(12) Vos, M. H.; Jones, M. R.; McGlynn, P.; Hunter, C. N.; Breton, J.; Martin, J.-L. *Biochim. Biophys. Acta* **1994**, *1186*, 117.
(13) Shreve, A. P.; Cherepy, N. J.; Franzen, S.; Boxer, G. S.; Mathies, R. A. *Proc. Natl. Acad. Sci. U.S.A.* **1991**, *88*, 11207.
(14) Palaniappan, V.; Aldema, M. A.; Frank, H. A.; Bocian, D. F. *Biochemistry* **1992**, *31*, 11050.
(15) Cherepy, N. J.; Shreve, A. P.; Moore, L. J.; Franzen, S.; Boxer, G. S.; Mathies, R. A. *J. Phys. Chem.* **1994**, *98*, 6023.
(16) Warshel, A. *Proc. Natl. Acad. Sci. U.S.A.* **1980**, *77*, 3105.
(17) Mukamel, S. In *Principles of Nonlinear Optical Spectroscopy*; Lapp, M., Ed.; Oxford University Press: Oxford, 1995.
(18) (a) Creighton, S.; Hwang, J.-K.; Warshel, A.; Parson, W. W.; Norris, J. *Biochemistry* **1988**, *27*, 774. (b) Warshel, A.; Chu, Z.-T.; Parson, W. W. *Science* **1989**, *246*, 112. (c) Parson, W. W.; Nagarajan, V.; Gaul, D.; Schenck, C. C.; Chu, Z.-T.; Warshel, A. In *Reaction Centers of Photosynthetic Bacteria*; Michel-Beyerle, M. E., Ed.; Springer: Berlin, 1991; p 239.
(19) (a) Treutlein, H.; Schulten, K.; Deisenhofer, J.; Michel, H.; Brunger, A.; Karplus, M. In *The photosynthetic bacterial reaction center: Structure and Dynamics*; Breton, J., Vermeglio, A., Eds.; Plenum: London, 1988; p 139. (b) Treutlein, H.; Schulten, K.; Brunger, A.; Karplus, M.; Deisenhofer, J.; Michel, H. *Proc. Natl. Acad. Sci. U.S.A.* **1992**, *89*, 75−79. (c) Tesch, M.; Schulten, K. *Chem. Phys.* **1991**, *158*, 421.
(20) Marchi, M.; Gehlen, J. N.; Chandler, D.; Newton, M. *J. Am. Chem. Soc.* **1993**, *115*, 4178.
(21) Warshel, A.; Chu, Z.-T.; Parson, W. W. *J. Photochem. Photobiol. A—Chem.* **1994**, *82*, 123.
(22) Gehlen, J. N.; Marchi, M.; Chandler, D. *Science* **1994**, *263*, 499.

an electronic transition involving the special pair, the bath ideally corresponds to the surrounding protein environment.

The underlying Hamiltonian of this simple model is a spin-boson Hamiltonian:

$$H = |\mathrm{g}\rangle H_\mathrm{g}\langle\mathrm{g}| + |\mathrm{e}\rangle\left\{H_\mathrm{e} - i\hbar\frac{\gamma}{2}\right\}\langle\mathrm{e}| + |\mathrm{g}\rangle H_\mathrm{ge}\langle\mathrm{e}| + |\mathrm{e}\rangle H_\mathrm{eq}\langle\mathrm{g}| \tag{1}$$

where H_α is the diabatic Hamiltonian of the state α (ground or excited), H_ge and H_eg are the interstate couplings, and γ is the inverse lifetime of the excited state. Only the diabatic Hamiltonians are relevant to electron−nuclear coupling. If the bath is harmonic, the H_g and H_e can be written as

$$H_\mathrm{g} = H_\mathrm{B}$$

$$H_\mathrm{e} = H_\mathrm{B} + U + \Delta G \tag{2}$$

where ΔG is the electronic energy difference between ground and excited states in the gas phase, H_B is a harmonic bath Hamiltonian, and U is a fluctuating field. Here, U can be represented by a linear combination of the harmonic modes of the bath which are linearly coupled to the electronic transition. The condition of a harmonic bath is not as restrictive as it might seems: only the degrees of freedom which are relevant to the electronic transition need obeying linear response.

The energy difference between state **g** and state **e**, the so-called energy gap, is a function of the nuclear coordinates and is directly related to the fluctuating field, indeed

$$\Delta E_\mathrm{eg} = U + \Delta G \tag{3}$$

Within the limit of the linear response model of eq 2, U is a Gaussian variable. The probability distributions of U in both states are themselves Gaussian. Consequently, the corresponding diabatic free energy surfaces are parabolic. That is

$$F_\mathrm{g} = \frac{1}{2c}U^2$$

$$F_\mathrm{e} = \frac{1}{2c}U^2 + U + \Delta G \tag{4}$$

Here, c is the curvature of the free energy surfaces. This curvature is related to the fluctuation of U, $u = U - \langle U\rangle$, according to

$$c = \beta\langle u^2\rangle \tag{5}$$

where $\beta = 1/k_\mathrm{B}T$ and $\langle ...\rangle$ indicate the equilibrium ensemble average.

Well-known expressions relate the dynamics of the energy gap, characterized by the time correlation function $\langle u(0)u(t)\rangle$, to the broadening of electronic bands.[17] In the next section we will show how to connect the time evolution of u to time-resolved stimulated emission experiments.

B. Stimulated Emission and Absorption. In a time-resolved stimulated emission experiment[23] the molecules contained in a specimen are photoexcited by a test beam of monochromatic light of frequency ω_1. At a variable time delay from the photoexciting beam a white light continuum probe beam is sent on the photoexcited sample. The intensity of the probe signal at a given wavelength ω_2 is measured and compared to the intensity of a reference beam which misses the specimen. The experiment measures the time-resolved transmission induced by the photoexciting beam of frequency ω_1 on the absorption at frequency ω_2. This transmission is then converted to absorption changes $\Delta A(t)$ defined as

$$\Delta A(t) = \ln\left(\frac{I_0(t)}{I(t)}\right) \tag{6}$$

where I_0 and I are respectively the intensity of the reference and the sample beam and t is the time elapsed from the initial excitation. The absorption change ΔA is proportional to the stimulated emission coefficient $S(\omega_1,\omega_2,t)$, which is the rate of emission of photons at frequency ω_2

$$\Delta A = -al\,S(\omega_1,\omega_2,t) \tag{7}$$

where l is the thickness of the sample and a is a positive coefficient which depends on characteristics of the sample, i.e. the concentration, etc.

Mukamel has shown that $S(\omega_1,\omega_2,t)$ can be expressed in the following form:[17,24]

$$\begin{aligned} S(\omega_1,\omega_1,t) = \int_{-\infty}^{t} dt_1 \int_{-\infty}^{t_1} dt_2 \int_{-\infty}^{t_2} dt_3\, F(t-t_3,t_1-t_3,t_2-t_3) \times \\ \psi(t-t_3,t_1-t_3,t_2-t_3)\,\phi(t_2)\,\phi^*(t_3) + F(t_1-t_3,t-t_3,t_2-t_3) \times \\ \psi(t_1-t_3,t-t_3,t_2-t_3)\,\phi(t_2)\,\phi^*(t_3) + F(t_2-t_3,t-t_3,t_1-t_3) \times \\ \psi(t_2-t_3,t-t_3,t_1-t_3)\,\phi(t_1)\,\phi^*(t_3) \end{aligned} \tag{8}$$

where $\phi(t)$ is the envelope of the electric field of the pump and

$$\psi(t_1,t_2,t_3) = \exp[-i\omega_1 t_3 - i\omega_2(t_1 - t_2) - \gamma/2(t_1 + t_2 - t_3)] \tag{9}$$

$F(t_1,t_2,t_3)$ is a four-point correlation function

$$F(t_1,t_2,t_3) = Tr[\mathrm{e}^{iH_\mathrm{e}t_1/\hbar}\mathrm{e}^{-iH_\mathrm{g}(t_1-t_2)/\hbar}\mathrm{e}^{-iH_\mathrm{e}(t_2-t_3)/\hbar}\mathrm{e}^{-iH_\mathrm{g}t_3/\hbar}\mathrm{e}^{-\beta H_\mathrm{g}}]/Q_\mathrm{g} \tag{10}$$

where Q_g is the partition function relative to the electronic ground state surface **g**. Using a cumulant expansion, the four-point correlation function can be expressed in terms of a function $g(t)$ which depends only on the fluctuation of the energy gap[25]

$$F(t_1,t_2,t_3) = \mathrm{e}^{i\omega_\mathrm{eg}(t_1-t_2+t_3)}\mathrm{e}^{[-g(t_1)+g(t_2)-g(t_3)-g(t_2-t_1)-g(t_3-t_2)+g(t_3-t_1)]} \tag{11}$$

where $\omega_\mathrm{eg} = \langle\Delta E_\mathrm{eg}\rangle_\mathrm{g}/\hbar$ and

$$g(t) = \frac{1}{\hbar^2}\int_0^t d\tau \int_0^\tau d\tau'\,\langle u(\tau')u(\tau)\rangle_\mathrm{g} \tag{12}$$

with $u(t) = \mathrm{e}^{iH_\mathrm{g}t/\hbar}u\mathrm{e}^{-iH_\mathrm{g}t/\hbar}$ and $u = U - \langle U\rangle_\mathrm{g}$. $\langle ...\rangle_\mathrm{g}$ denotes an average on the ground surface. If U is harmonic, the cumulant expansion gives an exact result.[17,25]

In an absorption experiment, things are simpler. When the sample is illuminated by a steady-state laser beam of frequency ω, the absorption change with respect to this reference beam is proportional to the absorption coefficient,

$$\Delta A = a'l\,\alpha(\omega) \tag{13}$$

As shown in refs 17 and 24, $\alpha(\omega)$ can be written in term of the function $g(t)$

$$\alpha(\omega) = Re\int_0^{+\infty} dt\,\mathrm{e}^{-i(\omega-\omega_\mathrm{eg})t-(\gamma/2)t}\mathrm{e}^{-g(t)} \tag{14}$$

(23) Martin, J.-L.; Migus, A.; Poyart, C.; LeCarpentier, Y.; Astier, R.; Antonetti, A. *Proc. Natl. Acad. Sci. U.S.A.* **1982**, *80*, 173.

(24) Mukamel, S. *J. Chem. Phys.* **1985**, *89*, 1077.

(25) Mukamel, S. *J. Chem. Phys.* **1982**, *77*, 173.

The function $g(t)$ appearing in the expressions for the four-point correlation function $F(t_1,t_2,t_3)$ and for $\alpha(\omega)$ can easily be obtained from the spectral density $J(\omega)$ or the Fourier transform of $\langle u(0)u(t)\rangle$

$$J(\omega) = \int_{-\infty}^{+\infty} dt\, e^{-i\omega t}\langle u(0)u(t)\rangle_g \qquad (15)$$

One has

$$g(t) = -\frac{1}{2\pi}\int_{-\infty}^{+\infty} d\omega\, \frac{J(\omega)}{(\hbar\omega)^2}(e^{i\omega t} - i\omega t - 1) \qquad (16)$$

A convenient semiclassical approximation to $J(\omega)$ which satisfy the detailed balance condition,[26] $J(-\omega) = e^{-\beta\hbar\omega}\, J(\omega)$, will be used throughout this work:

$$J_{sc}(\omega) = \frac{2}{1 + e^{-\beta\hbar\omega}} J_c(\omega) \qquad (17)$$

The dynamics of $S(\omega_1,\omega_2,t)$ depends on the fluctuating field $U(t)$ and on ω_2. When ω_2 is the frequency of the maximum of the emission peak, it corresponds to the average energy gap at the bottom of the diabatic surface of state **e**. Smaller or higher frequency corresponds to the turning point regions of the well. Probing the central region of the free energy well produces an essentially different oscillatory behavior of $S(\omega_1,\omega_2,t)$ with respect to the turning point regions. Here, the field passes twice for vibrational period in opposite directions, giving rise to all the harmonics of its fundamental frequencies.[10] Away from the bottom of the well, the dynamics of $S(\omega_1,\omega_2,t)$ tends to match that of the field, U.

In the preceding formulation, the reference Hamiltonian is H_g, i.e. the time evolution and the averages are carried out on the ground state surface. Since in the present study molecular dynamics was performed on the excited state, H_e must be considered as the reference Hamiltonian. We give the corresponding formulas for $S(\omega_1,\omega_2,t)$ and $\alpha(\omega)$ in the Appendix.

As a final remark, we would like to point out that our model for stimulated emission neglects contributions from nuclear tunneling effects which might be important at very low temperature. However, experiments conducted at different temperatures on *R. capsulatus* have shown that the essential oscillatory features of the time-dependent stimulated emission spectra are not qualitatively affected.[10]

III. Molecular Dynamics and Atomistic Model

A. Model Parameters. Our simulation is based on the X-ray structure of the photosynthetic reaction center of *Rb. sphaeroides* at 2.8 Å resolution taken from the Brookhaven data bank.[3] The terminal group subunits L, M, and H were obtained by replacing the amide and the carbonyl group respectively with a positively charged N-terminus and a negatively charged C-terminus. For each of the subunits the last amino acid with known X-ray position was chosen as the terminus.

The topology and the potential parameters of the amino acids forming the protein were taken from the united atom CHARMM force field,[27] which explicitly includes only the polar hydrogens. Since the atomic bonds were kept rigid, no stretching term was included in the potential energy function. The protonated state of all the amino acids were those at pH = 7, assuming standard pK values except for glutamate L104 which was protonated. A dielectric constant of 1 was used in all calculations.

In the past, Treutlein *et al.*[18a] have carried out a united atom parameterization of the bacteriochlorophylls and bacteriopheophytins of type *b* and of the quinones contained in the RC of *Rps. viridis*. Their potential parameters have the advantage of being compatible with the protein force field used in this study. Thus, although the chlorophylls contained in the RC of *Rb. sphaeroides* are of type *a*, in our simulation we have used Treutlein's potential model and have replaced the type *a* chlorophylls with type *b*. The electrostatic model for the excited state of the special pair P* will be described in detail in section IV.

B. RC Environment. Previous simulations have dealt with the RC environment by restraining the motion of part of the protein atoms and explicitly simulating only the atoms closer to the cofactors. These approaches ignore the natural surrounding of the RC.

Typically, RCs are embedded in a phospholipid bilayer (the cellular membrane) and surrounded on both sides by water solution (the cytoplasm and the peryplasm). Noticeably, RCs maintain their typical photosynthetic activity also outside of the bacteria environment. Indeed, many spectroscopic experiments are conducted in RCs in micellar solutions, in man-made membranes or in pellets. In the latter case, the RC proteins, depleted almost entirely of the detergent by chemical means, aggregate forming a hydrated precipitate. From a simulation point of view, the pellet environment is the simplest to study. It does not require the modeling of complicated membranes or large micelles and only involves simulating a hydrated RC. Consequently, we have chosen to simulate the RC of *Rb. sphaeroides* in this environment.

The initial atomic configuration for the system was prepared as follows: Firstly, the RC was placed in an orthogonal box of sides a = 65.63 Å, b = 58.0 Å, and c = 65.0 Å with its axis of quasi-symmetry parallel to the *a*-direction. Secondly, the box was filled with 9120 SPC[28] water molecules arranged in a simple cubic lattice. Thirdly, all the water molecules which had at least one atom within the van der Waals radius of any of the protein atoms were removed. The resulting system was composed of 8321 protein atoms and 4104 water molecules. Finally, to obtain electroneutrality, three water molecules picked at random were replaced by sodium cations.

C. Simulation Details. All the simulation runs of this study were carried out by using our in-house molecular dynamics program ORAC.[29] The equations of motion were numerically solved using a standard Verlet integrator.[30] The SHAKE bond constraint algorithm[31] was used to keep the SPC water molecules fully rigid and to maintain the protein atomic bonds to their X-ray values. In order to use a large integration step during the equilibration phase, the mass of the water and protein hydrogen were increased from 1.0 to 10.0 amu. A time step of 2.0 fs was used in this first stage. After equilibration, the hydrogen masses were reset and the integration time step decreased to 1.0 and 1.5 fs respectively for the runs at 300 and 50 K.

In order to perform the molecular dynamics simulation, a spherical cutoff of 9 Å was applied to the nonbonded interactions. A third-order spline function between 8 and 9 Å was used to eliminate the discontinuity in both the Lennard−Jones

(26) Borisow, J.; Moraldi, M.; Frommhold, L. *Mol. Phys.* **1985**, *56*, 913.

(27) Brooks, B. R.; Bruccoleri, R. E.; Olafson, B. D.; States, D. J.; Swaminathan, S.; Karplus, M. *J. Comput. Chem.* **1983**, *4*, 187. The united atom potential parameters CHARMM19 were used in our simulation.

(28) Berendsen, H. J. C.; Potsma, J. P. M.; Van Gunsteren, W. F.; Hermans, J. In *Intermolecular Forces*; Pullman, B., Ed.; Reidel: Dordrecht, Holland, 1981; p 331.

(29) Procacci, P.; Darden, T.; Paci, E.; Marchi, M. ORAC: A Molecular Dynamics Program to Simulate Complex Molecular Systems with Realistic Electrostatic Interactions. Submitted for publication to *J. Comput. Chem.*

(30) Verlet, L. *Phys. Rev.* **1967**, *159*, 98.

(31) Ryckaert, J. P.; Ciccotti, G.; Berendsen, H. J. C. *J. Comput. Phys.* **1977**, *23*, 327.

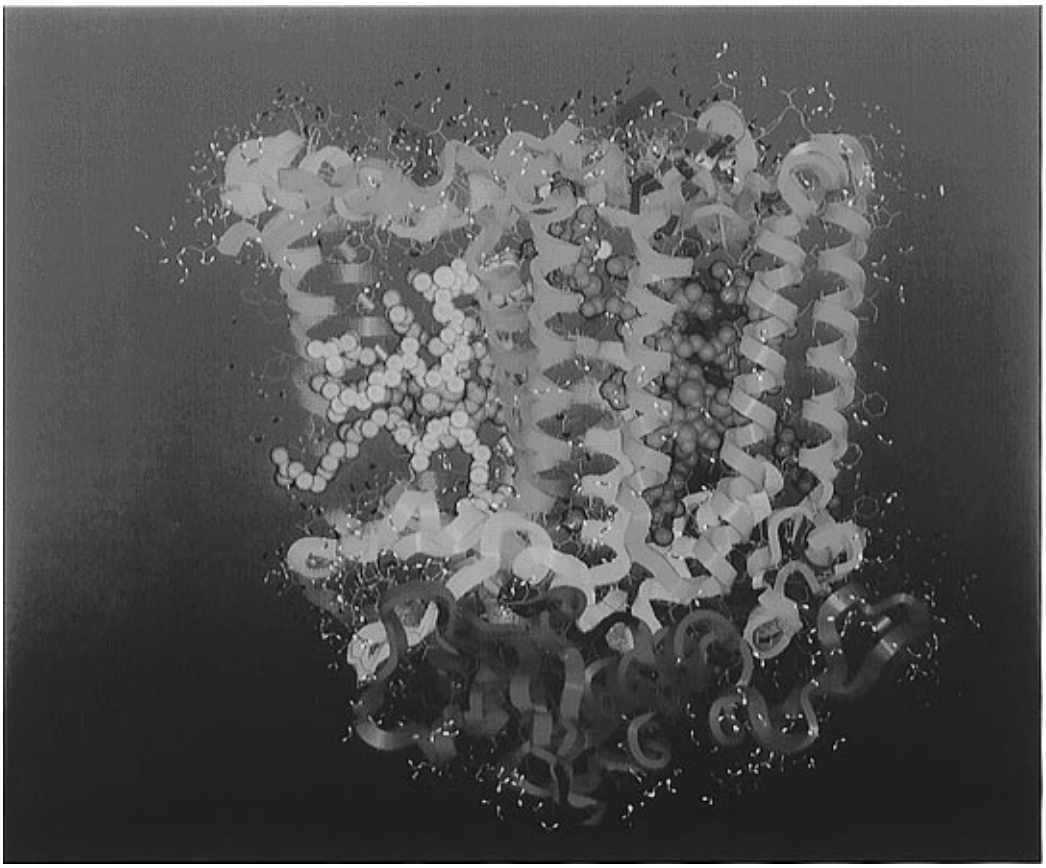

Figure 2. Snapshot of the reaction center of *Rhodobacter sphaeroides* after 130 ps of simulation. The backbones of the protein subunits L, M, and H are represented by ribbons respectively colored in green, light blue, and dark blue. The chromophores are found in the center of the protein colored in red for those on the L side and in yellow for those on the M side. Only the water molecules in the first solvation shell are shown in red and white.

and electrostatic potential function at the cutoff. It must be pointed out that spherical cutoff was applied only to the dynamics and not to the calculation of the energy gap (see section IV).

The RC in solution with the special pair in its ground state P was run at first without the sodium ions for 40.0 ps. Subsequently, the ions were included by replacing randomly three water molecules which were not bound to the protein surface. The system composed of the RC, the water molecules and the ions were further equilibrated for 89.0 ps more until the total potential energy had reached a plateau. In the equilibration the mass of the hydrogen was set to 10 amu and the time step to 2.0 fs. Before the acquisition run was begun, the hydrogen mass was reset to 1 amu, the time step decreased to 1.0 fs, and the system was equilibrated furtherly for 10 ps more. For all runs of this first stage, the temperature was kept around 300 K by reinitializing the velocities periodically. In Figure 2 we give a pictorial view of the RC protein and the first solvation shell water at the end of the equilibration period.

Data acquisition consisted of two runs. At first, we performed 100 ps of simulation at 300 K. Then, the electronic state was changed from P to P* and an additional equilibration was carried out for 15 ps, lowering the temperature to 50 K. At the same time, the time step was increased to 1.5 ps. Finally, the second data acquisition period was performed at 50 K for 90 ps.

During the first data acquisition period, instantaneous atomic configurations were collected every 75 fs to gather dynamical and structural information on the RC in solution. At the same time, time-dependent data on the energy gaps relevant to electron transfer were accumulated every 3 fs.

(32) Reference deleted in revision.

In the excited P* state at low temperature, the energy gap between the excited and ground states of the special pair was calculated and collected every two steps of simulation, i.e. 3 fs. As explained in detail in the next section, contributions from the first images of all the atoms of the RC, solvent, and ions were included in the energy gap calculation.

IV. Calculation of the Energy Gap

As in previous papers,[19,20,33] we assume that the electron involved in the excitation from P to P* interacts with the environment through a purely electrostatic pseudopotential. Thus, the diabatic free energies of the two states include only electrostatic contributions.

Although Stark spectroscopy has revealed that the excited state of P has a large permanent dipole moment,[34] the orientation of this dipole moment cannot be uniquely determined. However, based on findings of recent resonant Raman experiments[35] that the positive charge of the ionized P^+ is concentrated on P_M, it can be reasonably inferred that the P* state has a significant charge transfer character with a dipole moment oriented from P_M to P_L. Early semiempirical calculations[36] also support this supposition.

(33) (a) Kuharski, R. A.; Bader, J. S.; Chandler, D.; Sprik, M.; Klein, M. L.; Impey, R. W. *J. Chem. Phys.* **1988**, *89*, 3248. (b) Bader, J. S.; Chandler, D. *Chem. Phys. Lett.* **1989**, *157*, 501.

(34) Lockhart, D. J.; Goldstein, R. F.; Boxer, S. G. *J. Chem. Phys.* **1988**, *89*, 1408. Boxer, S. G.; Goldstein, R. A.; Lockhart, D. J.; Middendorf, T. R.; Takiff, L. *J. Phys. Chem.* **1989**, *93*, 8280−8294. Middendorf, T. R.; Mazzola, L. T.; Lao, K.; Boxer, S. G. *Biochim. Biophys. Acta* **1993**, *1143*, 223.

(35) Mattioli, T. A.; Hoffmann, A.; Sockalingum, D. G.; Schrader, B.; Robert, B.; Lutz, M. *Spectrochim. Acta* **1993**, *49A*, 785.

Instead of using electrostatic models proposed in the past for P*,[36] in this study we have chosen to use a simpler model. We have obtained P* from the ground state P, by uniformly redistributing 0.5 e^- from some selected atoms of P_L to the corresponding atoms on P_M. The 47 atoms involved in this charge exchange for each monomer were those belonging to the imidazole ring of the bacteriochlorophyll.

In order to compute the energy difference between a neutral and a charge transfer state, let us consider the two chromophores P_L and P_M composed of n_c charges interacting with the N_s charges of the environment composed of the RC and the water solution. The time-dependent positions of these charges are calculated by simulation. Let $\{q_i^{P_L\alpha}, q_i^{P_M\alpha}\}$ denote the charges of the chromophores in the electronic state α and $\{Q_i\}$ the charges of the environment. In the ground state $\alpha = 1$ while $\alpha = 2$ in the excited state.

Thus, the electrostatic energy of the state α is given by

$$E_\alpha = \sum_{i=1}^{n_c}\sum_{j=1}^{n_c}\frac{q_i^{P_L\alpha} q_j^{P_M\alpha}}{r_{ij}} + \sum_{i=1}^{n_c}\sum_{j=1}^{N_s}\frac{q_i^{P_L\alpha} Q_j}{r_{ij}} + \sum_{i=1}^{n_c}\sum_{j=1}^{N_s}\frac{q_i^{P_M\alpha} Q_j}{r_{ij}} + V_{self} \quad (18)$$

Here r_{ij} is the distance between the two charges, while V_{self} contains contributions from both interactions among charges belonging to the environment and among charges belonging to the same chromophore. It is clear that the former component is the same in both ground and excited state and cancels out in the calculation of the energy gap. The chromophore self energies are not included in our calculation. They should be part of the internal electronic energies of the bacteriochlorophylls which are not relevant to our calculation.

In our charge transfer model of the P* state, the excited state charges of each chromophore can be written as a function of its ground state charges

$$q_i^{P_L 2} = q_i^{P_L 1} + Q/n_c$$
$$q_i^{P_M 2} = q_i^{P_M 1} - Q/n_c \quad (19)$$

Where Q is the magnitude of the charge being transferred from the two bacteriochlorophylls.

Finally, by combining eqs 18 and 19, we obtain the following expression for the energy gap:

$$\Delta E_{eg} = E_2 - E_1 = \sum_{j=1}^{N_s} Q_j \left[\sum_{i\in P_L}^{n_c}\frac{Q/n_c}{r_{ij}} - \sum_{i\in P_M}^{n_c}\frac{Q/n_c}{r_{ij}}\right] + \sum_{i\in P_L}^{n_c}\sum_{j\in P_M}^{n_c}\frac{q_j^{P_M 1} Q/n_c - q_i^{P_L 1} Q/n_c - (Q/n_c)^2}{r_{ij}} \quad (20)$$

It is clear from the above equation that to calculate $\Delta E_{eg}(t)$ is sufficient to compute the average potential energy on the n_c sites of each chromophores (the first two terms in eq 20) and their instantaneous positions at time t. Thus, the energy gap is given as a sum of two components:

$$\Delta E_{eg} = \Delta E_{eg}^{S} + \Delta E_{eg}^{D} \quad (21)$$

Here, ΔE_{eq}^{S} and ΔE_{eg}^{D} are contributions respectively from the solvent environment (protein subunits and water) and from the bacteriochlorophyll dimer. While the former corresponds to the first term on the right hand side of eq 20, the latter includes the remaining terms.

(36) Plato, M.; Mobius, K.; Michel-Beyerle, M. E.; Bixon, M.; Jortner, J. *J. Am. Chem. Soc.* **1988**, *110*, 7279−7285. Scherer, P. O. J.; Fischer, S. F. *Chem. Phys.* **1989**, *131*, 115−127.

Table 1. Averaged x-RMS for the Three Subunits of the RC at 300 K[a]

subunit	α-carbon	heavy atoms	backbone atoms
L	2.04	2.32	2.00
M	1.99	2.30	1.95
H	2.72	3.01	2.67
total	2.23	2.52	2.18

[a] All values are in angstroms. See text for details.

V. Simulation Results

A. Protein Structure. Information about the structure of the RC in solution was obtained by analyzing 1000 protein + water configurations of the 300 K run.

Firstly, the X-ray coordinates of the RC were compared with the calculated average structure. To this purpose, for each coordinate configuration obtained in the simulation we minimized the root mean square difference between the coordinates of subunits L, M, and H and their X-ray counterpart (x-RMS), defined as

$$\text{x-RMS}_\alpha = \langle \min\left(\sum_{i\in\alpha}(\mathbf{r}_i - \mathbf{r}_i^X)^2\right)^{1/2}\rangle \quad (22)$$

Where α is the index of the protein subunit, $\mathbf{r}_i$ and $\mathbf{r}_i^X$ are respectively the atomic coordinates from the simulation and the X-ray. The symbol $\langle ... \rangle$ stands for average over the simulation ensemble.

In these minimizations only selected atoms were considered. In Table 1 we show the average x-RMS for the three subunits and the chromophores when the α carbon, backbone, and heavy atoms were included in the minimization. We found that our model of RC in solution reproduced well the experimental structure of the RC. The subunit H has the most disagreement. In Figure 3 the results concerning the C_α's of the three subunits are shown in details for each residue. It is found that the membrane-spanning helices of subunits L and M, labeled from A to E in the picture following ref 3, have a low value of x-RMS. The major disagreement in subunit L between calculated and experimental structure is near residue 60 in a region at the interface with water.

As a measure of the mobility of the protein atoms and of the solvation water, we calculated the root-mean-square displacement (RMS) from the average structure. The average RMS for the RC atoms was found to be 0.46 Å with no significant changes among different subunits. As expected, residues at the beginning or at the end of the subunits sequence were more mobile than the rest. In addition, the helices C in subunit M and A in subunit H were found to have an average RMS twice as large as the rest of the intermediate residues.

The head groups of the prosthetic molecules were found to be more rigid than the rest of the RC with a RMS 40% lower. On the contrary, the end of their hydrophobic tails was 5 times more mobile.

In order to investigate the structure of the solvent around the RC, we have further analyzed the coordinates accumulated during the run at 300 K. For each protein atom the first solvation shell was arbitrarily defined to include all the water molecules with at least one atom within 1.2 times the corresponding CHARMM van der Waals radius. In this framework, we found that, of the 4101 water molecules solvating the RC, 304 were bound to the protein for at least 90% of the time. Of these water molecules, respectively 78 and 103 were bound to

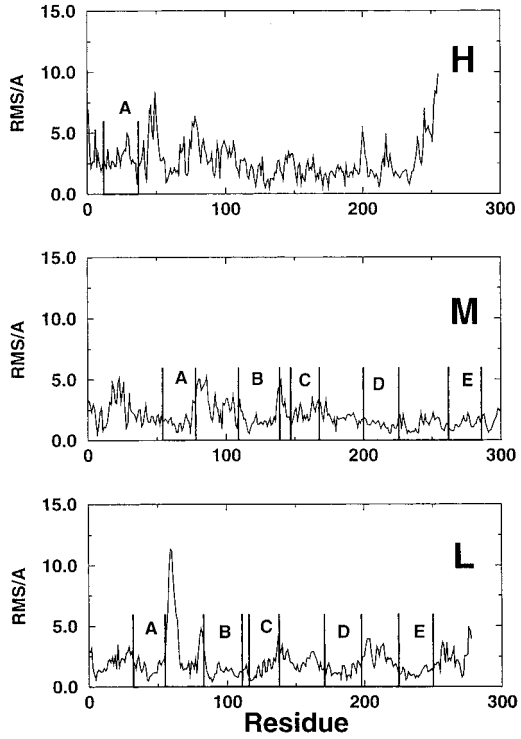

Figure 3. Root-mean-square difference between the calculated average structure and X-ray coordinates of subunits L, M, and H. The membrane-spanning region of each subunits are labeled with Roman letters from A to E following the convention in ref 3.

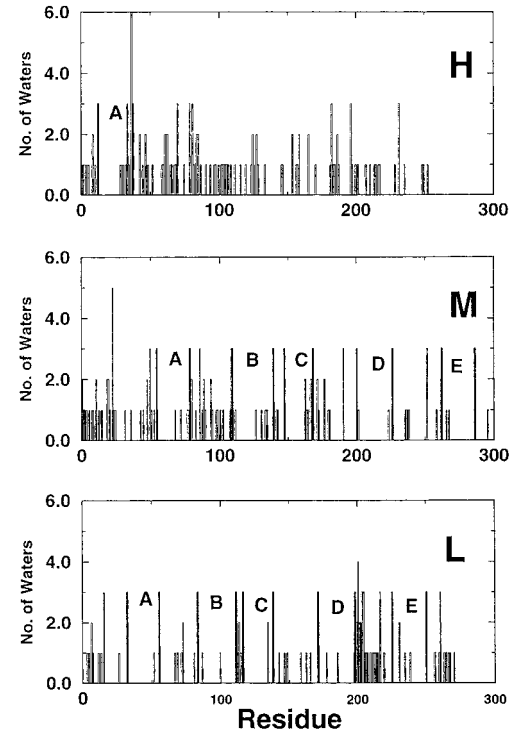

Figure 4. Number of bound water molecules versus the residue number of the three subunits. The membrane-spanning helices in each subunit are labeled in the same fashion as in Figure 3.

subunits L and M, while 123 were coordinated to subunit H. They are found most often in the hydrophilic region of the subunits. Many fewer are coordinated to residues in hydrophobic regions. This is shown in Figure 4 where a histogram of the number of bound waters versus the number of residue is shown for each subunits. It is noticeable that in the amino acids

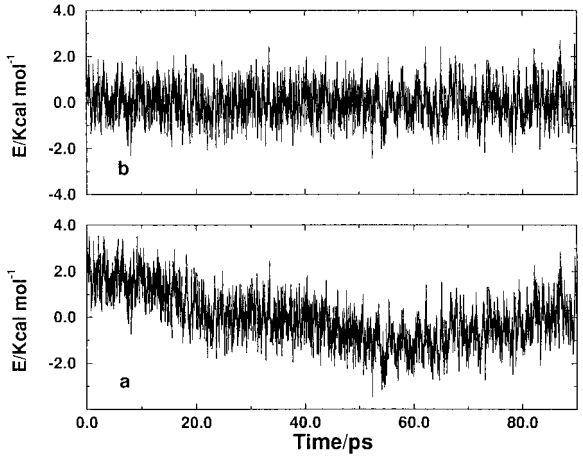

Figure 5. Energy gap versus simulation time: (a) as obtained in the equilibrium run at 50 K; (b) as obtained after filtering (see text for details).

belonging to the membrane-spanning helices the number of bound waters is significantly less than in the remaining residues.

B. Energy Gap Fluctuation. During the low-temperature run in the P* state, data regarding the energy difference between excited and ground state were accumulated for 90 ps. Our results in Figure 5a show the complex time-dependent behavior of the energy gap, ΔE_{eg}. Since the absolute value of the solvation energy for the charge transfer state is not relevant to our calculation, we show the fluctuation of the energy gap shifted to match the zero of the energy axis.

Visual inspection of Figure 5a indicates that the energy gap undergoes oscillations in time scales up to 120 ps. However only time scales 1 order of magnitude shorter can be accurately sampled by our simulation which is 90 ps long. Therefore, we have chosen to filter out vibrations with time period longer than 14 ps. It must be pointed out that stimulated emission experiments detect the slowest vibration with a time period of about 3 ps.

In order to filter out these low vibrations, we have subtracted to each data point in Figure 5a the running data average of length 14 ps centered on the point itself. Increasing or decreasing the running average to respectively 8 and 20 ps did not change significantly the position and the intensity of the peaks of the energy gap spectral density. In Figure 5b we present the filtered data.

In order to calculate the diabatic free energy surface for the stimulated emission discussed in section II.A, we first define the energy gap probability distribution as

$$P_{eg}(\epsilon) = \langle \delta(\Delta E_{eg} - \epsilon) \rangle \tag{23}$$

The corresponding diabatic free energy surface can be obtained from $P_{eg}(\epsilon)$ according to

$$F_{eg}(\epsilon) = -\beta \ln(P_{eg}(\epsilon)) \tag{24}$$

If ΔE_{eg} obeys Gaussian statistics, $P_{eg}(\epsilon)$ is a Gaussian and, consequently, $F_{eg}(\epsilon)$ is parabolic. In Figure 6 we show the results for $F_{eg}(\epsilon)$ obtained applying eqs 23 and 24 to the filtered trajectory in Figure 5b. Within statistical error, the calculated free energy surface can be interpolated by a parabola. Using higher order polynomial improves the fit of less than 1%. This finding is similar to previous results on electron transfer dynamics in liquids and in RCs.[20,33] Compared to the study in ref 20, the magnitude of the energy gap fluctuation we calculate for stimulated emission is one order of magnitude smaller, α being 0.753 kcal mol^{-1}.

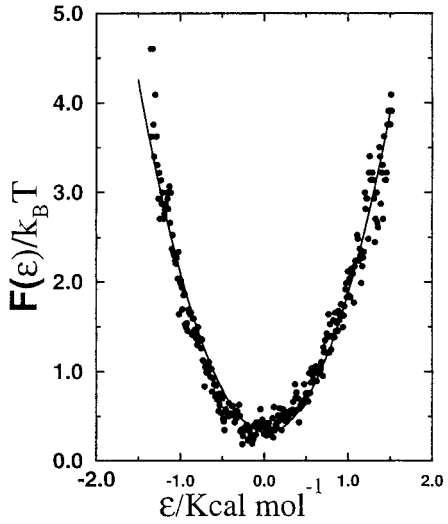

Figure 6. Energy gap free energy surface. The filled circles are results from the simulation at 50 K, while the continuous line is the quadratic fit.

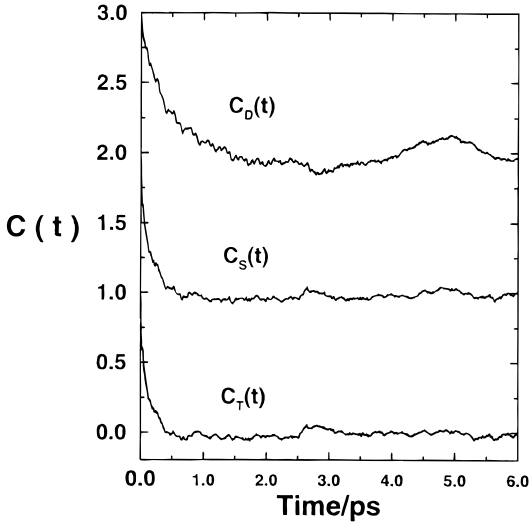

Figure 7. Comparison among the energy gap time correlation functions, $C_T(t)$, $C_S(t)$, and $C_D(t)$ between 0 and 6 ps. For clarity, the three correlation function are respectively shifted on the *y*-axis of 0.5 units.

C. Energy Gap Dynamics. Information regarding the energy gap dynamics can be gathered from the time correlation function of its fluctuations defined as

$$C(t) = \frac{\langle u(0)u(t)\rangle}{\langle u^2\rangle} \tag{25}$$

Where

$$u(t) = \Delta E_{eg}(t) - \langle \Delta E_{eg}\rangle \tag{26}$$

In Figure 7 we compare the time correlation function for the total energy gap, $C_T(t)$, with the corresponding functions for $\Delta E_{eg}{}^S$ and $\Delta E_{eg}{}^D$ (see section IV), respectively, called $C_S(t)$ and $C_D(t)$. Visual inspection reveals that the behavior of $C_T(t)$ and $C_s(t)$ are qualitatively similar and show many common oscillations, while in $C_D(t)$ low-frequency oscillations are enhanced.

At short times the $C_T(t)$ and $C_S(t)$ show an initial relaxation in the femtosecond time scale. Such a behavior is found also in $C_D(t)$, although the relaxation is slower and the function reaches its first minimum after 2.5 ps. Compared to the results on electron transfer dynamics in RCs,[20] the energy gap for the P* to P transition relaxes less rapidly. We find that $C_T(t)$ and $C_S(t)$ decay to their first minima after 500 fs, while the corresponding time for electron transfer is about 100 fs.

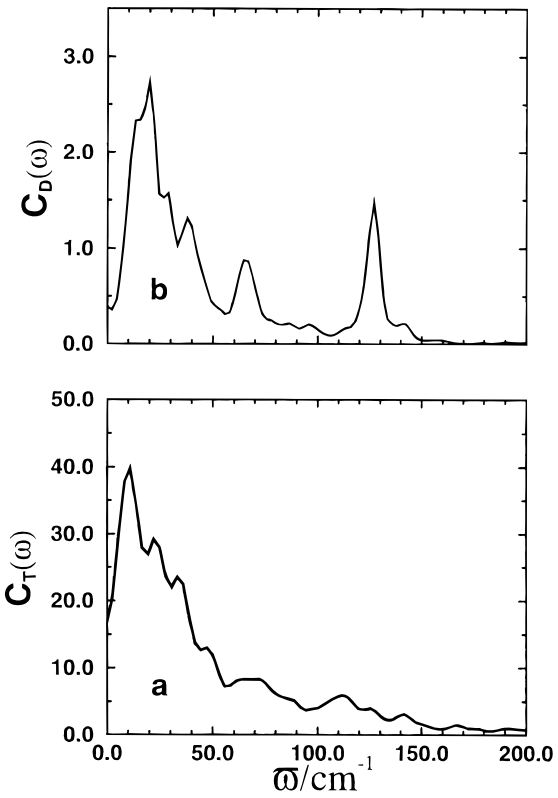

Figure 8. Comparison between the total spectral density in panel (a) and the contribution from the bacteriochlorophyll dimer in panel (b).

More interesting is the spectral density defined as

$$J(\omega) = \int_{-\infty}^{+\infty} \langle u(0)u(t)\rangle e^{-i\omega t}\, dt \tag{27}$$

In Figure 8 we show $J_S(\omega)$ and $J_D(\omega)$, respectively the contribution from the solvent and the dimer. In the low-frequency region below 50 cm^{-1} the two functions are almost identical both in the location of their peaks and relative intensities. At higher frequency $J_D(\omega)$ shows two enhanced peaks at 67 and 125 cm^{-1} which correspond to two broad bands in $J_S(\omega)$.

Thus, the comparison of the two spectral densities indicates that the nuclear vibrations coupled to the P* to P transition involve concerted motion between the solvent environment (protein and water) and the bacteriochlorophyll dimer. Although it is impossible to investigate the nature of the environment modes given the number and complexity of the nuclear coordinates involved, the analysis of the dimer trajectory is instead practicable.

D. Absorption. From the filtered energy gap data, we can now calculate the absorption. It is shown in Figure 9 with the stimulated emission. While the maximum of the absorption peak was set to 895 nm,[11] the emission peak was computed from $S(\omega_1,\omega_2,t)$ with $\omega_1 = 895$ nm and $t = 20$ ps. If before the excitation the system is at thermal equilibrium, the absorption peak corresponds to a transition between the bottom of surface **g** and the surface **e**. If t is large enough, the system becomes thermally averaged on the **e** surface and the maximum of stimulated emission corresponds to a transition between the bottom of the surface **e** and the surface **g**. Indeed, we checked that increasing t did not increase the shift of the emission spectrum with respect to the absorption peak. The width of

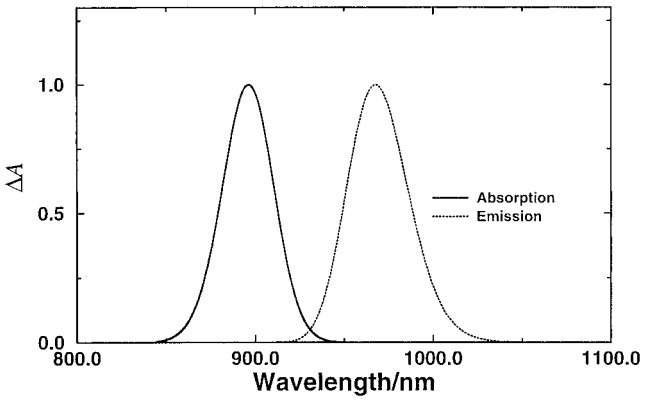

Figure 9. Normalized absorption and stimulated emission for $t = 20$ ps, from the equilibrium simulation run at 50 K. The position of the absorption and emission peaks is determined with an error on about ~5%.

both peak is ~400 cm^{-1}, which is smaller than the width of the experimental absorption peak (~500 cm^{-1}).[11] We stress that effects dues to inhomogeneity among RCs in the experimental sample were not accounted for in our calculation. Indeed we simulated only one RC.

E. Time-Resolved Stimulated Emission. For the sake of simplicity, we have calculated $S(\omega_1,\omega_2,t)$ defined by eq 8, using the following form for the envelope of the probe

$$\phi(t) = \begin{cases} 1 \text{ for } 0 \le t < 40 \text{ fs} \\ 0 \text{ else} \end{cases} \tag{28}$$

While the frequency of the pump, ω_1 was set to the maximum of the absorption peak, a set of probe frequencies was chosen which provided a coarse sampling of different regions of the emission band and allowed comparison with the time-resolved experiments. Four different probe wavelengths were considered: $\omega_2 = 968$ at the maximum of the emission band, $\omega_2 =$ 987 and 949 nm at half maximum from both sides of the emission peak, and, finally, $\omega_2 = 1003$ nm to sample a region far away from this maximum (see Figure 9).

The oscillatory part of $S(\omega_1,\omega_2,t)$, $H_{\omega_2}(t)$, is shown in Figure 10 for the four wavelengths. Away from the bottom of the free energy surface well ($\omega_2 = 968$ nm), $H_{\omega_2}(t)$ shows an oscillatory behavior, with a phase change of π between $\omega_2 = 987$ and 949 nm. Noticeably, at $\omega_2 = 968$ nm, the maximum of the emission peak, the aspect of $H_{\omega_2}(t)$ changes showing a decrease in the amplitude of the oscillations as well as the appearance of different oscillating features. For $\omega_2 = 1003$ nm, at the sides of the emission peak, $H_{\omega_2}(t)$ resembles very closely the energy gap time correlation function $C_T(t)$. Only at short times the two curves diverge. (See Figure 10a.)

For all wavelength, $H_{\omega_2}(t)$ shows coherent oscillations well beyond the 3 ps time mark. This contrasts with experimental results showing an exponential damping of the time correlation function within this time scale. Such a damping might be due to frictional damping or static disorder on the RCs. Noticeably, static disorder, corresponding to each special pair of the sample being in a slightly different environment, produces averaging of the energy gap spectral density or, equivalently, damping of the correlation function. Since in the simulation coherent oscillations persist until 10 ps, the special pair is not subject to high friction. Thus, our simulation seems to indicate that the experimental damping might be due only to static disorder.

Although $H_{\omega_2}(t)$ depends intimately on the energy gap autocorrelation function $C_T(t)$ (see section IIB), only at frequencies ω_2 far away from the emission peak and at long enough times do $H_{\omega_2}(t)$ and $C_T(t)$ overlap. This behavior is shown in

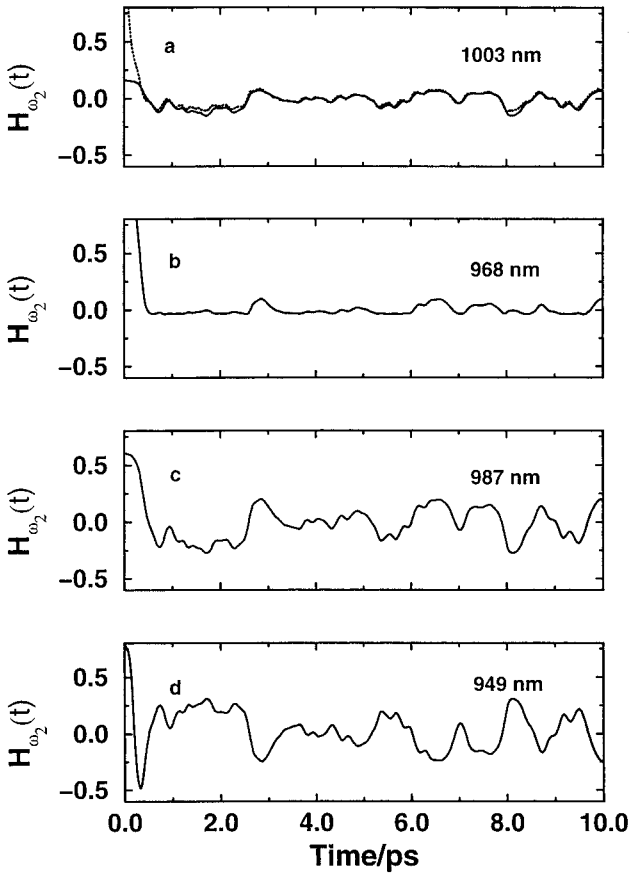

Figure 10. Oscillatory part of the calculated time resolved stimulated emission. As indicated in the figure, from top to bottom the four panels present results for ω_2 equal to respectively (a) 1003, (b) 968, (c) 987, and (d) 949 nm. For comparison, the autocorrelation function of the energy gap has been added on the panel (a) (dotted line). The statistical error is within three times the thickness of the lines.

Figure 10a where the two functions are compared. Because of the different behavior of $H_{\omega_2}(t)$ and $C_T(t)$ at short times, the dynamic information on the energy gap obtained from time-resolved experiments is incomplete.

Notwithstanding, a simple Fourier cosine transform of the time-resolved data can still provide all the relevant information on the position of the peaks of the energy gap spectral density and some information on their relative intensity. Indeed, let us consider a function $I_{\omega_2}(t)$ which is zero between t and Δt and equal to $H_{\omega_2}(t)$ at times farther than Δt,

$$I_{\omega_2}(t) = H_{\omega_2}(t) - \Pi_{\Delta t}(t)\, H_{\omega_2}(t) \tag{29}$$

where Δt is the time period during which $C_T(t)$ and $H_{\omega_2}(t)$ differ, such that

$$\Pi_{\Delta t}(t) = \begin{cases} 1 \text{ if } 0 \le t < \Delta t \\ 0 \text{ else} \end{cases} \tag{30}$$

The cosine Fourier transform of the expression (29) has the form

$$I_{\omega_2}(\omega) = H_{\omega_2}(\omega) - \Pi_{\Delta t}(\omega) \bigstar H_{\omega_2}(\omega) \tag{31}$$

where ★ denotes convolution, $\Pi_{\Delta t}(\omega) = 2 \sin(\omega \Delta t)/\omega$ and $I_{\omega_2}(\omega)$ is the reduced spectrum.

While $\Pi_{\Delta t}(\omega)$ can be interpreted as a frequency window of width $\Delta\omega$ directly related to Δt, its convolution product $\Pi_{\Delta t}(\omega) \bigstar H_{\omega_2}(\omega)$ at each frequency ω corresponds to a weighted average of $H_{\omega_2}(\omega)$. Thus, the suppression of the data in time domain between 0 and Δt is equivalent in the frequency domain

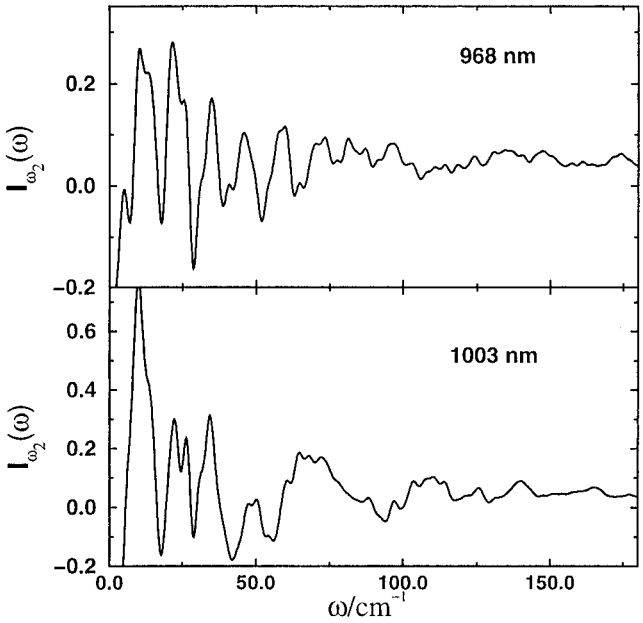

Figure 11. Reduced spectral density of the computed time resolved stimulated emission, for $\omega_2 = 1003$ and 968 nm. $\Delta t = 0.5$ ps was used (see text for details).

to removing from $H_{\omega_2}(\omega)$ its average weighted by the frequency window $\Pi_{\Delta t}(\omega)$. Spectral oscillations in the frequency domain on scales lower than $\Delta\omega$ will remain on the resulting spectrum.

In practice, typical Δt's of time-resolved experiments are in the order of a few hundreds of femtoseconds which correspond to $\Delta\omega$'s of 40 cm^{-1} and larger. In this case, the reduced spectrum $I_{\omega_2}(\omega)$ will show peaks at the same frequencies as those found in the energy gap spectral density. Unfortunately, the information on the peak relative intensity will be incomplete. Although the above arguments are valid only for time-resolved experiments far away from the emission peak, for consistency, we compute the reduced spectra also for all the other probe frequencies data.

The spectra $I_{\omega_2}(\omega)$'s calculated at two wavelengths, $\omega_2 =$ 1003 and 968 nm, are shown in Figure 11. A $\Delta t = 0.5$ ps was chosen since at shorter times, $H_{\omega_2}(t)$ calculated for $\omega_2 = 1003$ nm and $C_T(t)$ begin differing from each other. The width of the corresponding frequency window was then equal to 40 cm^{-1}. The reduced spectra were also convoluted with a Lorentzian function of hwhm = 1.8 cm^{-1}, which is the Fourier transform of $e^{-t/\tau}$ where $\tau = 3$ ps.

At $\omega_2 = 1003$ nm, $I_{\omega_2}(\omega)$ shows peaks at 10, 22, 26, and 35 cm^{-1}, a structured peak at 50 cm^{-1} and weak shoulders at 70 and 110 cm^{-1}. At $\omega_2 = 968$ nm, a new peak appears at 5 cm^{-1} and the peak at 50 cm^{-1} splits into two peaks at 46 and 60 cm^{-1}. Moreover, the region after 60 cm^{-1} is more structured than for $\omega_2 = 1003$ nm. This increase of the number of peaks can be interpreted as due to the appearance of harmonics and combinations of the fundamental frequencies. The experimental spectra shows similar behavior[9,10] when the maximum of emission peak is probed.

In past experiments,[9,10] information regarding the frequency and intensity of the energy gap oscillations were extracted by plotting the squares of the Fourier coefficients of the time-resolved spectra. In this study, the Fourier analysis described above was applied also to the experimental data. The reduced spectrum obtained from the time-resolved experimental data at $\omega_2 = 938$ nm (shown in the inset) is shown in Figure 12 for Δt = 0.3 ps. Such a Δt suppresses the first negative oscillation of $H_{\omega_2}(t)$ and corresponds in the frequency domain to a window

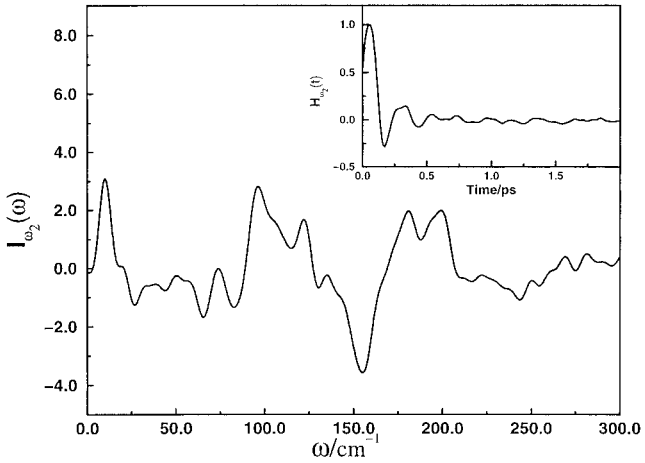

Figure 12. Reduced spectral density of the experimental time resolved stimulated emission data of ref 11. $\Delta t = 0.5$ ps was used (see text for details). The oscillatory part of the experimental time-resolved stimulated emission is shown in the inset.

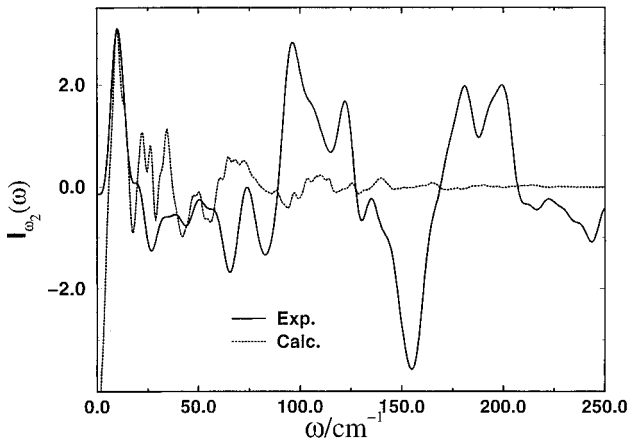

Figure 13. Comparison between the experimental and calculated reduced spectral densities. The two spectra are normalized with respect to the intensities of their lowest frequency peak.

of width $\Delta\omega = 67$ cm^{-1}. Thus, oscillations in the reduced spectrum on a frequency scale lower than 67 cm^{-1} are not an artifact of the pump−probe technique. Such oscillations correspond to prominent peaks at 10, 74, 96, 122, 135, 181, and 199 cm^{-1}. Two structured peaks appear also at ∼39 and ∼50 cm^{-1}.

The peaks obtained by our spectral analysis of the experimental data differ somewhat from those obtained by Vos *et al.*[11] In particular, the peak at 153 cm^{-1} is a minimum of our reduced spectrum while the peaks at 135 and 181 are not visible in Vos's results.

In Figure 13 the experimental and calculated $I_{\omega_2}(\omega)$ are compared by normalizing the intensities of their respective lowest frequency peaks. No visible intensity is found in the computed spectrum beyond the weak band at 110 cm^{-1}, while the experiment shows intense modes at frequencies higher than 135 cm^{-1}. In addition, although the calculation reproduces the first experimental peak at 10 cm^{-1}, the activities of the higher frequency modes is underestimated with respect to experiment. This result and the finding on section V.C that the higher frequency peaks (at 67 and 125 cm^{-1}) in the dimer energy gap spectral density are weaken considerably by solvent effects might suggest the our simple electrostatic model underestimates the dimer−solvent energy gap with respect to the intradimer counterpart.

VI. Conclusion

This paper has focused on issues related to the coupling mechanism between nuclear modes and electronic emission in the bacterial reaction center of *Rb. sphaeroides*. We have reported results for the hydrated reaction center studied by molecular dynamics simulation technique. The RC was simulated with full periodic boundary conditions and immersed in a box of 4101 water molecules. At 300 K the protein average structure was found in reasonable agreement with the X-ray data. Remarkably, our hydration of the RC did not affect significantly the structure of the membrane-spanning helices of the subunit L and M which showed a low root mean square differences from their X-ray coordinates.

The main result of this study has stemmed from the simulation at 50 K carried out with the special pair bacteriochlorophyll dimer in its excited state and is summarized by Figure 12. We have modeled the photoemission P* to P with a two-level system coupled linearly to a fluctuating field representative of some of the nuclear degrees of freedom of the protein environment. Using this simple model, our study has been able to reproduce some features of the experimental time-resolved spectra and has also discriminated between contributions to the spectra deriving from the protein environment and from interdimer interactions. In particular, we have found the lowest frequency oscillations in the same time scale as in the experiment. These oscillations along with the others at higher frequency have corresponding excitations in the interdimer dynamics as shown in Figure 8. This finding can provide means to ascertain the nature of the nuclear vibrations by analyzing further the MD trajectory of the special pair in order to determine the quasi-normal modes corresponding to each vibrations. This is the aim of an undergoing investigation.

Our simulation has also shown that the time-resolved emission spectrum does not experience frictional damping and coherent oscillations persist for up to ~10 ps. This is in contrast with experiments on a variety of *R. sphaeroides* mutants[11] and suggests that static disorder might be responsible of the experimental damping occurring within 3 ps.

Future work will address the issue of improving the potential model for the ground and excited state of P. This includes input from accurate quantum chemical calculations on bacteriochlorophylls and incorporation of polarization effects in the model. Also, the role of nonlinear effects on the dielectric response should be investigated. Hopefully, these improvements in the theoretical model will make possible a more quantitative study of the system.

In conclusion, this paper has shown that classical molecular dynamics simulation combined with a simple model for electronic transition is capable of providing an useful picture of the medium dielectric response even in systems as complex as membrane proteins.

We hope that, with this approach, issues related to the dielectric asymmetry of RCs[37] and, therefore, to the more general problem of the primary electron transfer asymmetry could soon be tackled.

Acknowledgment. We would like to thank Marten Vos for the numerous discussions about his experiments and for providing us his digitized experimental results. Stimulating conversations about infrared and Raman spectroscopy with Marc Lutz, were beneficial.

(37) Steffen, M. A.; Lao, K. Q.; Boxer, S. G. *Science* **1994**, *264*, 810.

Appendix

It was shown in section II.B how to compute the absorption and emission spectra from the knowledge of the energy gap dynamics on the ground state. If instead, as it is the case of this study, the time evolution of the energy gap is known on the excited states, the four-point correlation function $F(t_1,t_2,t_3)$ must be rewritten in term of averages on the excited state surface, **e**. This can be easily done by replacing in eq 10 the identities

$$e^{-iH_g t/\hbar} = e^{-iH_e t/\hbar} \exp_+\left[\frac{i}{\hbar}\int_0^t U_e(\tau)\, d\tau\right] \tag{32}$$

$$e^{iH_g t/\hbar} = \exp_-\left[-\frac{i}{\hbar}\int_0^t U_e(\tau)\, d\tau\right] e^{iH_e t/\hbar} \tag{33}$$

and

$$e^{-\beta H_g} = \exp_-[\int_0^\beta d\alpha\, U_e(i\alpha\hbar)] e^{-\beta H_e} \tag{34}$$

where $\exp_-$ and $\exp_+$ are time-ordered exponential[17,24,25] and $U_e(t) = e^{iH_e t/\hbar} U e^{-iH_e t/\hbar}$ with $U = H_e - H_g$.

After a cumulant expansion, one obtains

$$F(t_1,t_2,t_3) = \frac{Q_e}{Q_g} e^{i\omega'_{eg}(t_1-t_2+t_3-i\beta\hbar)} \times e^{[-g_e^\star(t_1)+g_e^\star(t_2)-g_e^\star(t_3)-g_e(t_2-t_1)-g_e(t_3-t_2)+g_e(t_3-t_1)]} \times e^{f_e(t_1)-f_e(t_2)+f_e(t_3)} e^{g_e(i\beta\hbar)} \tag{35}$$

Where the superscript ★ denotes complex conjugate, Q_e is the partition function relative to the excited potential energy surface, and $\omega'_{eg} = \langle \Delta E_{eg} \rangle_e$. In addition,

$$g_e(t) = \frac{1}{\hbar^2}\int_0^t d\tau \int_0^\tau d\tau' \langle u_e(\tau') u_e(\tau)\rangle_e \tag{36}$$

$$g_e(i\beta\hbar) = \int_0^\beta d\alpha \int_0^\alpha d\alpha' \langle u_e(i\alpha'\hbar) u_e(i\alpha\hbar)\rangle_e \tag{37}$$

and

$$f_e(t) = \frac{i}{\hbar}\int_0^t d\tau \int_0^\beta d\alpha \langle u_e(\tau) u_e(i\alpha\hbar)\rangle_e \tag{38}$$

with $u_e(t) = e^{iH_e t/\hbar} u e^{-iH_e t/\hbar}$.

It can be easily shown that $f_e(t)$ can be expressed in terms of the spectral density of the energy gap:

$$f(t) = \frac{1}{2\pi}\int_{-\infty}^{+\infty} d\omega \frac{J(\omega)}{(\hbar\omega)^2}(1 - e^{-\beta\hbar\omega})(1 - e^{-i\omega t}) \tag{39}$$

Using the same procedure, one can find a new form for the absorption coefficient which contains only averages on the excited state, i.e.

$$\alpha(\omega) = \frac{Q_e}{Q_g} Re \int_0^{+\infty} dt\, e^{-i(\omega-\omega'_{eg})t-(\gamma/2)t+\beta\hbar\omega'_{eg}} e^{-g_e^\star(t)+f_e(t)+g_e(i\beta\hbar)} \tag{40}$$

JA943841C